Acta Pharmaceutica Sinica B 2020;10(8):1534–1548

Chinese Pharmaceutical Association
Institute of Materia Medica, Chinese Academy of Medical Sciences

Acta Pharmaceutica Sinica B

www.elsevier.com/locate/apsb
www.sciencedirect.com

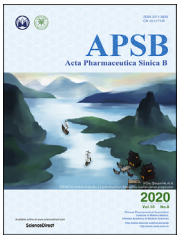

ORIGINAL ARTICLE

Doxorubicin-loaded bacterial outer-membrane vesicles exert enhanced anti-tumor efficacy in non-small-cell lung cancer

Kudelaidi Kuerban[a,b,†], Xiwen Gao[a,†], Hui Zhang[a,b], Jiayang Liu[a,b], Mengxue Dong[a,b], Lina Wu[c], Ruihong Ye[d], Meiqing Feng[a,b], Li Ye[a,b,*]

[a]*Minghang Hospital & Department of Biological Medicines at School of Pharmacy, Fudan University, Shanghai 201100, China*
[b]*Shanghai Engineering Research Center of ImmunoTherapeutics, School of Pharmacy, Fudan University, Shanghai 201203, China*
[c]*TOF-PET/CT/MR Center, the 4th Affiliated Hospital, Harbin Medical University, Harbin 150028, China*
[d]*Department of Pharmaceutical Engineering, School of Pharmacy, Hubei University of Chinese Medicine, Wuhan 430070, China*

Received 13 November 2019; received in revised form 29 December 2019; accepted 2 January 2020

KEY WORDS

Bacterial outer-membrane vesicles;
Doxorubicin;
Non-small-cell lung cancer;
Anti-tumor efficacy;
Chemoimmunotherapy

Abstract More efficient drug delivery system and formulation with less adverse effects are needed for the clinical application of broad-spectrum antineoplastic agent doxorubicin (DOX). Here we obtained outer-membrane vesicles (OMVs), a nano-sized proteoliposomes naturally released by Gram-negative bacteria, from attenuated *Klebsiella pneumonia* and prepared doxorubicin-loaded O0MVs (DOX-OMV). Confocal microscopy and *in vivo* distribution study observed that DOX encapsulated in OMVs was efficiently transported into NSCLC A549 cells. DOX-OMV resulted in intensive cytotoxic effects and cell apoptosis *in vitro* as evident from MTT assay, Western blotting and flow cytometry due to the rapid cellular uptake of DOX. In A549 tumor-bearing BALB/c nude mice, DOX-OMV presented a substantial tumor growth inhibition with favorable tolerability and pharmacokinetic profile, and TUNEL assay and H&E staining displayed extensive apoptotic cells and necrosis in tumor tissues. More importantly, OMVs' appropriate immunogenicity enabled the recruitment of macrophages in tumor microenvironment which might synergize with their cargo DOX *in vivo*. Our results suggest that OMVs can not

*Corresponding author. Tel.: +86 21 5198 0035; fax: +86 21 5198 0036.
E-mail address: yelil@fudan.edu.cn (Li Ye).
†These authors made equal contributions to this work.
Peer review under responsibility of Institute of Materia Medica, Chinese Academy of Medical Sciences and Chinese Pharmaceutical Association.

https://doi.org/10.1016/j.apsb.2020.02.002

only function as biological nanocarriers for chemotherapeutic agents but also elicit suitable immune responses, thus having a great potential for the tumor chemoimmunotherapy.

1. Introduction

According to the report of Global Cancer Statistics 2018, lung cancer is the leading cause of cancer incidence (11.6% of the total cases) and mortality (18.4% of the total cancer deaths) worldwide. In China, lung cancer is also the cancer with the highest morbidity and mortality in both sexes combined[1]. The most frequent type of lung cancer is non-small cell lung cancer (NSCLC) which comprises 85% of all lung cancer. In recent years, immunotherapy and targeted therapy have made significant contributions to the improved treatment of NSCLC. However, combined chemotherapy is still the first-line therapy approach for the patients diagnosed with stage IV NSCLC[2].

Doxorubicin (DOX), belonging to the anthracyclines family, has proven to be one of the most effective and widely used antineoplastic agents. As a frontline chemotherapy drug, DOX has been used for the treatment of various cancers including lung cancer. The main mechanism of its antitumor effect is that DOX inhibits topoisomerase types I and II, and intercalates into DNA, inducing DNA breaks. Unfortunately, it non-specifically targets at all kind of cells resulting in many life-threatening adverse effects such as cardiotoxicity, myelosuppression and immunosuppression, which limits its clinical application[3]. Various drug delivery systems, especially DOX-loaded liposomes, have been developed to enhance permeability and selectivity, and prolong circulation time, thereby alleviating the cytotoxicity to normal tissues[4]. The pegylated liposomal DOX, Doxil, is the first liposomal drug and nano-drug approved by FDA (November 17, 1995) which exerts comparable efficacy to DOX with obviously reduced cardiotoxicity[5]. Depending on the enhanced permeability and retention (EPR) effect, Doxil can be targeted passively to tumors and demonstrates relatively higher drug concentrations in tumors as compared with that in adjacent normal tissues. But for all these advantages, the application of Doxil has not been prevalent in the clinic due to the skin toxic effect as well as the lower bioavailability[6,7]. Furthermore, the *in vivo* accumulating toxicological effect of liposomes should not be ignored[8]. More efficient drug delivery systems combined with low cytotoxicity are constantly being pursued to improve the usefulness of DOX.

Recently, biological nanocarriers derived from bacteria, virus and mammalian cells have received extensive attention, as they are biodegradable and have evolved specific functions *in vivo* such as prolonged circulation through evading the immune system and selective targeting that are often desired in drug delivery system[9]. Outer-membrane vesicles (OMVs) are nano-sized (20−250 nm in diameter), bilayered and spherical proteoliposomes enriched with outer membrane and periplasmic content, and detach consistently from the envelope of Gram-negative bacteria during their growth[10]. OMVs facilitate bacteria to communicate with their environment through acting as transportation system. In the host, OMVs can fuse with host cells and deliver content into the cytosol[11]. Their significant role in biological processes such as intercellular communication, adherence and colonization to different hosts has attracted considerable attention for the study as specialized drug delivery carriers[12].

OMVs carry plenty of immune stimulators that can activate the host immune system *in vivo*[13]. This natural feature is utilized in immunotherapy, with applications ranging from vaccines to cancer therapy[14,15]. A vaccine containing OMVs from *Neisseria meningitides* had been approved by the European Commission to be used in individuals older than 2 months, and over 80 million doses further reassured its safety[16,17]. So far, OMVs have been used as delivery vectors for proteins, plasmid, small interfering RNA, and other therapeutic agents. However, there are only a few studies in which OMVs simply act as carriers and their immune capacity is not utilized[18]. It is commonly believed that bacteria as well as their derived products are pathogenic, which restricts their clinical application for safety concern. Nevertheless, also the expert thinks that the reservation of immunogenicity to certain degree can be helpful especially for the cancer immunotherapy, because of OMVs' adjuvant ability[9].

In the present study, we utilized OMVs from attenuated *Klebsiella pneumonia* to prepare doxorubicin-loaded OMVs (DOX-OMVs). Its cytotoxicity and apoptosis effects on NSCLC A549 cells were compared with free DOX and doxorubicin-loaded liposomes (DOX-LIPOs) *in vitro* and *in vivo*. In addition, pharmacokinetics, safety evaluation as well as immune responses were investigated. Our data suggest that DOX-OMVs not only facilitate the accumulation of chemotherapeutic drugs in tumor tissue but also induce appropriate anti-tumor immune responses, thereby producing enhanced anti-tumor effect on NSCLC.

2. Materials and methods

2.1. Regents, antibodies and animals

Doxorubicin hydrochloride (DOX) was obtained from Shanghai Shifeng Biological Technology Co., Ltd. (Shanghai, China). Other reagents were obtained as listed below: 3-(4,5-dimetrylthiazol-2-yl)-2,5-diphenyltetrazolium bromide (MTT; Sigma−Aldrich, St. Louis, MO, USA); BCA protein assay kit and Annexin V-FITC/PI apoptosis detection kit (NanJing KeyGen Biotech Co., Ltd., Nanjing, China); TUNEL assay kit (Roche, Oceanside, CA, USA); PVDF transfer (Merck Millipore, Darmstadt, Germany); trypsin−EDTA solution, phenylmethanesulfonyl fluoride (PMSF) and RIPA lysis buffer (Shanghai Beyotime Biotechnology, Shanghai, China); EDTA (pH 9.0) antigen repair buffer, hematoxylin and proteinase K stock solution (Servicebio, Wuhan, China); diaminobenzidine developer (DAKO, Agilent, Santa Clara, CA, USA); all antibodies (caspase3, GAPDH, PARP, tubulin, F4/80) and HRP-conjugated secondary antibody were provided by Cell Signaling Technology (Danvers, MA, USA). Mouse IL-6/TNF-α/IFN-γ uncoated ELISA were obtained from Thermo Fisher Scientific Inc. (Waltham, MA, USA).

Male New Zealand white rabbits (2.0 ± 0.2 kg), 6-week-old female C57BL/6 mice and BALB/c nude mice (18−20 g) were provided by Animal Experimental Center, Fudan University

(Shanghai, China). All animal experiments were approved by Experimental Animal Ethics Committee of School of Pharmacy Fudan University (Shanghai, China).

2.2. Isolation, purification and characterization of OMVs[19]

Attenuated *K. pneumonia* ACCC 60095 was purchased from Agricultural Culture Collection of China, Beijing, China. Nasal drop experiment in mice was performed to demonstrate the safety of this strain. BALB/c mice underwent nasal administration of attenuated *K. pneumonia* and its OMVs with normal saline as negative control and pathogenic strain as positive control once a day for 10 days. Then, lung tissues were removed for H&E staining. For OMV preparation, *K. pneumonia* was inoculated into sterilized 1000 mL of LB broth and incubated overnight at 37 °C and 180 rpm (Gyrotory Tier Shaker, New Brunswick Scientific, Edison, NJ, USA). The culture was centrifuged at 4 °C and 5000×*g* (Anke, Shenzhen, China) for 30 min to obtain the supernatant, followed by further filtration with 0.22 μm filters (Pall Life Science, New York, NY, USA) to remove parental bacterial debris and other contaminants. The supernatant was further concentrated to 1/8 of its initial volume using 100 KDa ultrafiltration membranes (Millipore Amicon, Darmstadt, Germany) and ultracentrifuged at 4 °C and 60,000×*g* (Hitachi C21G, HITACHI, Maru, Chiyoda, Tokyo, Japan) for 30 min, and washed with phosphate buffer saline (PBS) twice to obtain the crude OMVs. The purified OMVs were obtained by ultracentrifugation at 4 °C and 300,000×*g* (Hitachi C21G) for 2 h using a sucrose density gradient, followed by removal of endotoxin using Detoxi-Gel Endotoxin Removing Columns (Thermo Scientific, Waltham, MA, USA). The concentration of OMVs was determined by BCA protein assay (Multiskan go, Thermo Scientific). To observe the morphology and size of OMVs, a drop of isolated OMVs solution was placed on copper grid. The dried grid containing OMVs was stained with a 2% of phosphotungstic acid solution (*w/w*, pH 7.1) and visualized using a JEM 1410 transmission electron microscope (JEOL, Peabaody, MA, USA). Also, dynamic light scattering (Zetasizer Nano zs, Malvern, Netherlands) was used to measure the size. OMVs were filtered through 0.22 μm filters and stored at −80 °C until use.

2.3. Loading therapeutic cargo

To prepare DOX-loaded OMVs (DOX-OMV), DOX and OMVs were gently mixed in PBS at an appropriate mass ratio, and then incubated at 37 °C for 4 h. To remove free DOX from DOX-OMV and to concentrate, 100 kDa ultrafiltration membranes were utilized. The obtained DOX-OMVs were then washed several times with PBS to ensure most free DOX was eliminated (Heraeus Multifuge X1R, Hanau, Germany). The concentration of DOX encapsulated in OMVs (encapsulation efficiency) was measured using LC−MS (Agilent Technologies, Santa Clara, CA, USA) with Agilent SB-C18 column (3.0 mm × 50 mm, 1.8 μm), 40% methanol and 60% water containing 1% formic acid as mobile phase, flow rate at 0.25 mL/min and detection wave length at 560 nm. Again, dynamic light scattering technology and transmission electron microscope were used to observe the morphology and size of DOX-OMV. The DOX-OMVs were filtered through 0.22 μm filter to eliminate bacteria. Drug release study *in vitro* was carried out in pH7.4 PBS containing 1% (*v/v*) Tween 80 which simulated the environment of blood system. The DOX-OMV solution was put into the dialysis bag (MWCO: 3500). Next, the dialysis bag was placed in 200 mL of PBS, and then shake incubated at 100 rpm (Decolorization shaker TS-II, Orbital Shakers, Atkinson, NH, USA) and 37 °C. At different time points, the PBS was sampled for analysis of drug concentration by LC−MS.

2.4. Cell culture

The NSCLC A549 cell line, as well as murine Ana-1 cell line were purchased from Cell Bank of Chinese Academy of Sciences, Shanghai Branch (Shanghai, China), and cultured in RPMI-1640 medium (CORNING, Corning, NY, USA) added with 10% of fetal bovine serum (Gibco, Carlsbad, CA, USA), penicillin (100 IU/mL) as well as streptomycin (100 μg/mL) at 37 °C in a CO_2 (5%) incubator (Thermo Scientific).

2.5. Cytotoxicity on A549 cells in vitro

The cytotoxic effect of DOX-OMV was quantitatively evaluated by the colorimetric, tetrazolium-based MTT assay. A549 cells (5×10^3 cells/well) were seeded into 96-well plates and incubated overnight, then treated with free DOX, DOX encapsulated in OMVs (DOX-OMV), DOX encapsulated in liposome (DOX-LIPO) and empty OMVs at a series of concentration gradients for 24 h 10 μL of MTT solution (concentration 5 mg/mL) was added to each well and incubated for 4 h at 37 °C and then the medium containing MTT was removed. The formazan product was dissolved by adding 100 μL of dimethyl sulfoxide (DMSO) to each well. The plates were read at 570 nm using a microplate reader (Multiskan Go, Thermo Scientific) and cell viability was calculated as the percentage of viable cells in the treated groups compared to the control group.

2.6. Western blotting

After treated with indicated concentrations of OMVs, DOX-OMV or free DOX for 24 h, the cells were collected and washed three times with PBS, and then lysed thoroughly in RIPA lysis buffer for more than 30 min at 4 °C and centrifuged for 5 min at 12,000×*g* (TGL-20 B, Shanghai Anting Scientific Instrument Factory, Shanghai, China) to obtain the supernatant. Equal amounts of total protein in lysates (20 μg) were separated by SDS-PAGE and then electrotransferred to polyvinylidene fluoride (PVDF) membranes. The PVDF membranes were blocked by incubating with 5% BSA for 2 h in TBST, and then incubated with primary antibodies at 4 °C overnight. Thereafter, they were incubated with HRP-conjugated secondary antibodies for 2 h at room temperature. The immunoblots were visualized using ECL chemiluminescence detection kit (Pierce, Rockford, IL, USA). The protein bands were quantified by using ImageJ software (National institutes of Health, Bethesda, MA, USA).

2.7. Confocal microscopy

Lipophilic tracer, 3,3′-dioctadecyloxacarbocyanine perchlorate (DiO, Invitrogen, Carlsbad, CA, USA) was adopted to label OMVs, and confocal microscopy was used to detect the cellular uptake of drug. A549 cells were seeded into confocal dishes (NEST Biotechnology, Wuxi, China), cultured overnight and then treated with OMVs, DOX (20 μg/mL), 20 μg/mL of DOX loaded in OMVs (DOX-OMV) or loaded in liposome (DOX-LIPO) separately for 12 h, or incubated with DOX-OMV for 0, 6, 12 and 24 h separately. Hoechst 33,342 dye was used to stain the nucleic acid of live cells. Fluorescence microscopy measurements were

conducted on a Zeiss Observer (Zeiss, Germany) using a dark field and fluorescence channels (excitation wavelength/emission wavelength: 480 nm/594 nm for doxorubicin, 484 nm/501 nm for DiO, 350 nm/461 nm for Hoechst 33,324). Images were processed using ZEN software (Zeiss microscopy, White Plains, NY, USA).

2.8. Flow cytometry

Cell apoptosis was detected by using Annexin V-FITC/PI detection kit. Cells were adjusted to 5×10^5/mL and treated with OMVs, DOX (20 μg/mL), 20 μg/mL of DOX loaded in OMVs (DOX-OMV) or loaded in liposome (DOX-LIPO) separately. After treated for 24 h, cells were collected and washed with PBS, followed by dispersion into staining solution with PI and Annexin V at concentration suggested by manufacturer. Cells were assayed using a flow cytometer (Becton−Dickinson, Fullerton, CA, USA) after co-staining at room temperature for 15 min under dark condition.

2.9. Anti-tumor effect and drug distribution in vivo

A549 cells (1×10^6/mL) were injected subcutaneously into the right flank of BALB/c nude mice (18−20 g). When the average tumor size reached 50 mm^3, the mice were divided randomly into 5 groups to receive daily intraperitoneal injection of the following treatments: (a) vehicle control (PBS); (b) free DOX (2 mg/kg); (c) 2 mg/kg of DOX loaded into OMVs; (d) 2 mg/kg of DOX loaded into liposomes; (e) empty OMVs. Tumors were measured every day, and tumor volumes were calculated from tumor length (L) and width (W) according to Eq. (1):

$$\text{Tumor volume} = \left(L \times W^2\right) / 2 \quad (1)$$

Eleven days later, the mice were subjected to dissection, and the tumors as well as the main organs were removed for various analyses. The blood sample was also collected for biochemical detection. For drug *in vivo* distribution study, mice bearing A549 tumors (~100 mm^3) were injected a single dose of free DOX (2 μL/g), equivalent DOX loaded into OMVs or loaded into liposomes. At 1, 4 and 9 h, mice were selected randomly to obtain tumors and major organs for the investigation of DOX distribution and tumor targeting through *ex vivo* fluorescence imaging (IVIS Lumina imaging system, Waltham, MA, USA). The fluorescence intensity of DOX in each organ was calculated for the biodistribution analysis by Living Image version 4.3.1 (Caliper Life Science, Inc., Waltham, MA, USA).

2.10. Immune cytokine analysis

C57BL/6 mice were used to investigate *in vivo* immune responses. The experiment designed the groups and dosage regimen as above. Blood samples were collected at 1, 3, 6, 24 and 48 h after initial administration, as well as day 11 of treatment. The respective ELISA kits were adopted to analyze the level of serum cytokines such as IL-6, TNF-α and interferon (IFN)-γ in accordance with the manufacturer's instructions. For investigation of *in vitro* immune activation, murine Ana-1 cells were treated with OMVs, DOX (20 μg/mL), 20 μg/mL of DOX loaded in OMVs (DOX-OMV) separately for 12 h. The release of cytokines was also detected using ELISA kits.

2.11. Histology and immunohistochemistry

Tumor and organ tissues were paraffin-embedded and sectioned into 4 μm after fixed in 4% of paraformaldehyde solution for 24 h. The sections were deparaffinized and rehydrated before detection. For histological observation, tumor sections were stained with hematoxylin and eosin (H&E), and then observed by an inverted microscopy (Nikon, Japan).

For immunohistochemistry analysis, the sections were treated with 3% hydrogen peroxide for 30 min to block endogenous peroxidase, and then incubated with F4/80 glycoprotein primary antibody for overnight at 4 °C. Thereafter, the slides were treated for 1.5 h with secondary antibody at room temperature. After washing with PBS, the sections were incubated for 10 min with 3,3′-diaminobenzidine (DAB) chromogenic solution followed by washing in PBS. The sections were counterstained with hematoxylin after DAB coloration. The antibody specificity was confirmed by negative control without primary antibody treatment. Immunopositive areas were observed by an inverted microscope (Nikon, Japan).

2.12. TUNEL assay

The deparaffinized and rehydrated tumor sections were permeabilized with proteinase K for 30 min, washed with PBS, and then treated with TUNEL assay kit according to the manufacturer's instructions. After the sections were developed by DAB chromogenic solution and counterstained with hematoxylin, the apoptosis of tumor tissues was detected by fluorescence microscopy (Nikon, Japan).

2.13. Pharmacokinetics

Nine rabbits were divided randomly into three groups: DOX group, DOX-LIPO group and DOX-OMV group. Plasma values of DOX equivalents administered i.v. to rabbits at a dose of 1.0 mg/kg of free DOX, DOX entrapped in liposomes and DOX encapsulated in OMVs were applied to obtain the pharmacokinetic parameters. Blood samples were taken intravenously into anticoagulant tubes at 0, 1, 2, 4, 6, 12 and 24 h after drug administration. After centrifugation at 2500 rpm (TGL-20 B) for 10 min, the obtained plasma was mixed with bacterial lysis buffer (Thermo Fisher Scientific,1:9, *v*/*v*) and ultrasonically treated for 5−10 min, and then centrifuged at 60,000×*g* (Hitachi C21G) for 15 min to obtain supernatant. Thereafter, the plasma concentrations of DOX were detected by LC−MS as described above. The data were calculated using DAS 2.0 software (DAS Development Group, BioGuider Co., Shanghai, China) for pharmacokinetic parameters. For the detection of DOX released from DOX-OMV in plasma *in vivo*, the plasma samples without bacterial lysis buffer treatment were processed by 100 kDa ultrafiltration membranes, then the ultrafiltrate was sampled for DOX concentration analysis by LC−MS.

2.14. Statistical analysis

Statistical analysis was carried out by GraphPad Prism 6.0. All data were expressed as mean ± SD. The data of deferent groups were compared using One-way ANOVA analysis. Values of $P < 0.05$ were regarded as statistically significant.

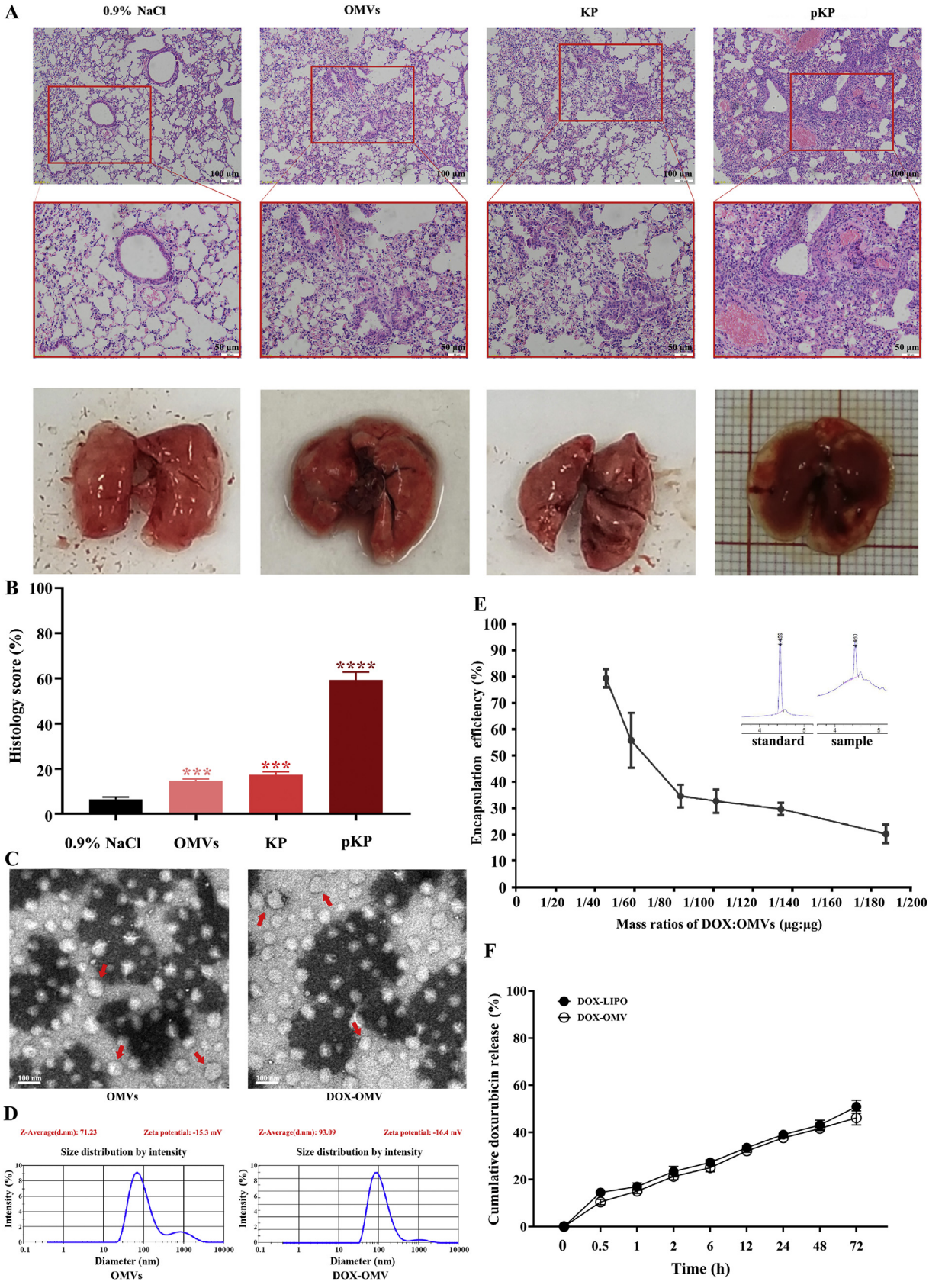
A
0.9% NaCl
OMVs
KP
pKP
100 μm
50 μm
B
Histology score (%)
0.9% NaCl
OMVs
KP
pKP
****
***
***
C
OMVs
DOX-OMV
D
Z-Average(d.nm): 71.23
Zeta potential: -15.3 mV
Size distribution by intensity
Intensity (%)
Diameter (nm)
OMVs
Z-Average(d.nm): 93.09
Zeta potential: -16.4 mV
Size distribution by intensity
Intensity (%)
Diameter (nm)
DOX-OMV
E
Encapsulation efficiency (%)
standard
sample
Mass ratios of DOX:OMVs (μg:μg)
F
DOX-LIPO
DOX-OMV
Cumulative doxurubicin release (%)
Time (h)

3. Results

3.1. Preparation and characterization of DOX-OMV

In this study, OMVs were prepared from attenuated *K. pneumonia* through multiple centrifugation and ultrafiltration steps, and further purified using density gradient centrifugation and endotoxin-removing columns[19,20]. Nasal drop experiment in mice demonstrated that this strain and its OMVs had very low virulence (Fig. 1A and B). Transmission electron microscopic analysis observed the spherical nanostructure of OMVs (Fig. 1C). Dynamic light scattering (DLS) measurement showed a relatively narrow particle size distribution (polydispersity index 0.212), and the average diameter of OMVs was 71.23 nm (Fig. 1D). These characteristics were consistent with previous observations of typical OMVs[20]. We subsequently obtained DOX-loaded OMVs (DOX-OMV) through co-incubation of OMVs and DOX in appropriate proportions, followed by ultrafiltration to eliminate free DOX. The electron micrograph in Fig. 1C displays that the encapsulation of DOX did not alter the uniform characteristics of OMVs, while the average diameter of DOX-OMV increased to 93.09 nm (Fig. 1D). Meanwhile, the quantity of DOX in OMVs and the encapsulation efficiency (EE) was analyzed using LC−MS. The results in Fig. 1E indicate that the encapsulation efficiency decreased obviously as the mass ratios of DOX:OMVs increased. We then adopted the mass ratios of 1:45 (DOX:OMVs) to prepare DOX-OMV in the following study for the encapsulation efficiency reached above 78%.

In order to check the stability of DOX-OMV, drug release study was carried out *in vitro*, indicating that the release rate of DOX encapsulated in OMVs was below 30% of the total entrapped drug being released within 6 h, followed by a relatively slow release over 48 h (Fig. 1F). We also prepared doxorubicin-loaded liposomes (DOX-LIPO) as comparison, and the electron micrograph and DLS measurement results were presented in Supporting Information Fig. S1.

3.2. Drug uptake by tumor cells

To determine whether OMVs could deliver effectively DOX to NSCLC cells *in vitro*, A549 cells were treated with OMVs, free DOX, and an equivalent dose of DOX encapsulated into either OMVs or liposomes for 12 h separately. Confocal microscopy showed the cellular uptake of drug, in which the blue and green fluorescence represented the location of cell nuclei and OMVs respectively, and the red was the intrinsic fluorescence of DOX. Although DOX could enter the cells by passive diffusion, which could accumulate in the nucleus by the preferred binding ability of DOX to DNA[3], little DOX fluorescence was observed in free DOX treated cells. This phenomenon may be due to a relatively small amount of DOX diffused into the cells, as well as the lower intensity of intrinsic fluorescence as compared with fluorescent dyes[21]. By contrast, the enhanced red fluorescence appeared in both DOX-OMV and DOX-LIPO treated cells, demonstrating that the drug uptake was improved after DOX was loaded into OMVs or liposomes. Moreover, the colocalization (yellow) of the OMVs (green) and DOX (red) was observed in DOX-OMV treated tumor cells, suggesting that OMVs carried DOX invading cells (Fig. 2A).

For DOX loaded into OMVs, the uptake increased gradually with the treatment time growing. At 6 h, the OMVs and DOX were mainly colacalizated on the cell membrane with a small amount of entry into the cells. At 12 h, a great deal of DOX was transported into cells by OMVs. After 24 h treatment, an intensified red fluorescence in the cell nuclei indicated that massive DOX entered into nuclear compartments (Fig. 2B and C). In addition, electron microscopy of A549 cells treated with DOX-OMV for 12 h displayed possible intracellular OMVs in and around vacuoles, which was consistent with the findings reported by Kesty et al.[22] about the *Escherichia coli* derived OMV entry into eukaryotic cells (Fig. 2D). Furthermore, *ex vivo* fluorescence imaging manifests that DOX encapsulated in OMVs accumulated rapidly in tumor tissues and displayed strong fluorescence signals at 1 h following a sustained retention within 9 h after administration, while presented a lower level of DOX distribution in main organs especially in the heart as compared with free DOX treated mice (Fig. 2E and F).

Altogether, both *in vitro* and *in vivo* experiments elucidated the advantage of OMVs to improve the transportation of DOX into the tumor cells.

3.3. Antitumor effect of DOX-OMV in vitro

To quantitatively evaluate the anti-NSCLC efficacy of DOX-OMV *in vitro*, MTT assay was carried out, and the results seem promising. Cytotoxic effect of DOX-OMV on A549 cells were increased compared to DOX itself at the same dosage and it was comparable to the cytotoxic effect of DOX-LIPO (Fig. 3A). The data were analyzed using Graphpad Prism software, and the half maximal inhibitory concentration (IC_{50}) were 35.51, 12.19 and 11.92 μg/mL, respectively, for DOX, DOX-LIPO and DOX-OMV. The effect of empty OMVs was also evaluated and the results indicated that OMVs had no obvious effect on cell viability.

DOX can induce caspase-dependent apoptosis through the activation of various molecular signals from AMPK (AMP-activated protein kinase)[3]. We then investigated the apoptosis-inducing effect of DOX-OMV on A549 cells by detecting the activation of caspase 3 and the downstream key protein PARP. Cells administered with indicated concentrations of OMVs, free DOX or DOX encapsulated in OMVs were analyzed by Western blotting. The results in Fig. 3B reveal that DOX-OMV led to more

Figure 1 Preparation and characterization of DOX-OMV. (A) Virulence of attenuated *K. pneumonia* ACCC 60095 and its OMVs. BALB/c mice underwent nasal administration of attenuated *K. pneumonia* (KP) and its OMVs with normal saline as negative control and pathogenic strain (pKP) as positive control once a day for 10 days. Lung tissues were removed for H&E staining. Scale bar = 100 μm (upper), 50 μm (lower). (B) Histology score evaluation of H&E staining by ImageJ software. Data are mean ± SD, $n = 3$; $^{***}P < 0.001$, $^{****}P < 0.0001$ *vs.* negative control. (C) Transmission electron micrographs of OMVs prepared from attenuated *K. pneumonia* and DOX-loaded OMVs (DOX-OMV). Arrows indicated typical OMVs and DOX-OMV. Scale bar = 100 nm. (D) Size distribution profile of OMVs and DOX-OMV. (E) The encapsulation efficiency (EE) analyzed by LC−MS. Data are mean ± SD, $n = 3$. (F) Time course of DOX release from DOX-OMV. Data are mean ± SD, $n = 3$. Drug release study *in vitro* was carried out in pH7.4 PBS containing 1% (*v*/*v*) Tween 80. The DOX-OMV solution was put into the dialysis bag. Next, the dialysis bag was placed in 200 mL of PBS, and then shake incubated at 100 rpm and 37 °C. At different time points, the PBS was sampled for analysis of drug concentration.

cleavage of caspase 3 and PARP than free DOX at the same dosage, and the apoptosis-inducing effect was dose-dependent. Cell apoptosis was further confirmed by flow cytometry analysis. As shown in Fig. 3C, both DOX-OMV and DOX-LIPO initiated an increased percentage of apoptotic cells as compared with free DOX and empty OMVs.

All of these data suggested that DOX-OMV could facilitate the cellular uptake of drug and then induce tumor cell apoptosis more effectively.

3.4. *Antitumor efficacy of DOX-OMV in vivo*

Subsequently, we assessed the capacity of DOX-OMV to inhibit tumor growth *in vivo*. The xenotransplanted tumor model of human NSCLC was established by subcutaneously injecting A549 cell line in nude mice. After tumor volume reached ~50 mm^3, tumor-bearing mice were randomly assigned into five groups, and injected i.p. with sterile PBS, empty OMVs, DOX-OMV, DOX-LIPO and an equivalent dose of free DOX separately. There was no significant fluctuation in the body weight of mice under all experimental conditions used (Supporting Information Fig. S2), and all treatments did not resulted in lethality. A pronounced inhibition of tumor growth was observed in the mice treated with DOX-OMV and DOX-LIPO after 11 days' treatment for the tumors almost disappeared in these two groups. In addition, DOX encapsulated in OMVs was able to take effect more quickly than that encapsulated in liposomes (Fig. 4A and B). TUNEL assay observed a large amount of apoptotic cells in tumor tissues collected from the mice treated with DOX-OMV, DOX-LIPO and OMVs, while the groups treated with free DOX presented the lowest level of green fluorescence (Fig. 4C and D). Moreover, histological analyses of tumor sections indicate that DOX-OMV and DOX-LIPO triggered extensive tumor necrosis, and free DOX and empty OMVs could also induce somewhat tumor necrosis as compared with the control (Fig. 4E).

It was noteworthy that empty OMVs also presented more efficient anti-tumor activity than free DOX *in vivo*, which was different from the *in vitro* experimental results. It is well known that OMVs can modulate the host immune response and facilitate the activation of innate and adaptive immunity[14], thus we speculated that OMVs might induce innate immune response in tumor-bearing nude mice. The immunohistochemistry staining by F4/80 antibody verified this hypothesis. The F4/80 glycoprotein is one of the most specific surface biomarkers for murine macrophages[23,24]. The results in Fig. 4F and G show an up-regulated F4/80 protein expression level in the tumor tissues of both OMVs and DOX-OMV treated mice, indicating the accumulation of macrophages in tumor microenvironment. Moreover, MTT assay indicated that OMVs had no obvious toxic effects on macrophages (Supporting Information Fig. S3).

3.5. *Investigation of immune response triggered by DOX-OMV*

Furthermore, we investigated whether the administration of DOX-OMV could trigger adaptive immune response in mice. *In vitro*, both OMVs and DOX-OMV could induce macrophages releasing TNF-α and IL-6 (Supporting Information Fig. S4). *In vivo* immune responses were detected in C57BL/6 mice during repeated administration of either DOX, OMVs, DOX-LIPO or DOX-OMV. At the first 1−3 h of the initial treatment, OMVs/DOX-OMV treatment groups showed remarkable increases in serum TNF-α and IL-6 levels as compared with DOX/DOX-LIPO treatment groups, which gradually down-regulated with time went on, and IL-6 returned to nearly basic levels at 24 h (Fig. 5A). In addition, we also observed that, after 11 days of administration, the serum levels of TNF-α, IL-6 and IFN-γ maintained at low levels in all groups, while OMVs/DOX-OMV treatment groups displayed relatively higher levels than other groups (Fig. 5B). The initial obvious upregulation in cytokine levels upon treatments with OMVs and DOX-OMV might be ascribed to the enriched proteins and LPS in OMVs which can induce the systemic cytokine release. However, the subsequent downgrade of serum cytokine levels suggested that DOX-OMV did not trigger severe inflammatory cytokine response, thereby could be well tolerated. Moreover, the appropriate upregulation of host immune responses might help to exert anti-tumor immunological effect.

3.6. *Safety evaluation of DOX-OMV*

Cardiac toxicity is the most severe dose-limiting adverse effect of DOX. We then investigated whether DOX-OMV therapy could ameliorate or avoid cardiac damage. After 11-day of treatment, the tumor-bearing mice were sacrificed and blood samples were obtained for detecting the markers of cardiac toxicity such as lactate dehydrogenase (LDH), aspartate aminotransferase (AST) and creatine kinase/MB isoenzyme (CK-MB). The activities of AST and CK-MB were remarkably lower in the serum of OMVs and DOX-OMV treated-mice as compared with free DOX treated-mice, and were close to those of control group (Fig. 6A). The values of LDH were somewhat higher in the serum of OMVs and DOX-OMV treated-mice than in the serum of control mice, but were lower than those of free DOX and DOX-LIPO treated mice. These findings are accorded with the results from *in vivo* drug distribution study that free DOX accumulated a lot in the heart, while DOX-OMV targeted effectively to the tumor (Fig. 2E and F). Therefore, DOX-OMV had less cardiotoxicity than free DOX.

We also carried out histological examination of heart, liver, spleen, lung and kidney from mice. Hematoxylin and eosin (H&E) staining results show that OMVs and DOX-OMV treated-mice had no obvious damage in these tissues as compared with the control group. However, there are some lesions in these tissues such as alveolar injury, cell apoptosis and minimal hemorrhage in free DOX and DOX-LIPO treated-mice, with the heart and lung more obvious (Fig. 6B). All of these data suggest that OMVs were safe and effective delivery carriers for tumor chemotherapy drugs.

3.7. *In vivo pharmacokinetic studies of DOX-OMV*

The plasma values of DOX equivalents administered to rabbits at a dose of 1.0 mg/kg i.v. of free DOX, DOX-OMV and DOX-LIPO are applied to obtain the pharmacokinetic parameters, and the results are presented in Fig. 7 and Table 1. Following a single dose administration, DOX-OMV displayed the slowest decay in plasma concentration of drug than OMVs and DOX-LIPO. Free DOX was cleared from blood very rapidly, and the half-life in initial distribution phase ($t_{1/2\alpha}$) was about 2 h. In contrast, DOX-OMV administration produced the initial half-life ($t_{1/2\alpha}$) of 4.177 h, which is 2-fold higher than free DOX. The rate of clearance of free DOX was 1.536 mL/h/kg compared to 0.786 mL/h/kg with DOX-OMV. The area under the blood concentration−time curve for free DOX, DOX-LIPO and DOX-OMV were 684.125, 936.594 and 1234.364 (mg h/L). In addition, the concentration of DOX released from DOX-OMV in plasma samples from DOX-OMV treated group was very low (Supporting Information

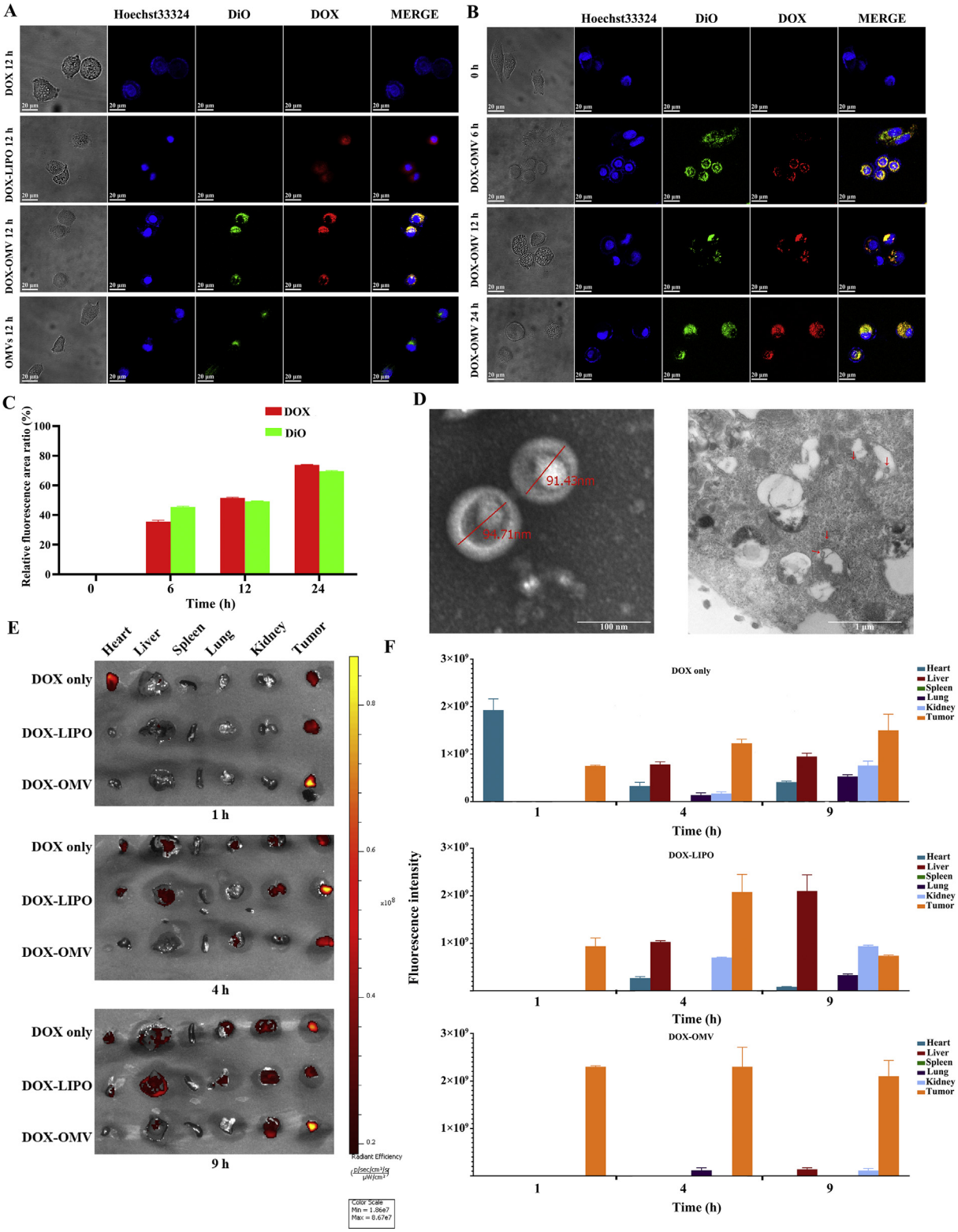

Figure 2 Drug uptake by tumor cells. (A)−(C) Cellular uptake of DOX detected by confocal microscopy. A549 cells were treated with (A) OMVs, DOX (20 μg/mL), 20 μg/mL of DOX loaded in OMVs (DOX-OMV) or loaded in liposome (DOX-LIPO) separately for 12 h or (B) DOX-OMV for 0, 6, 12 and 24 h. OMVs were labeled with DiO (green fluorescence). The blue fluorescence represented the location of cell nuclei and the red was the intrinsic fluorescence of DOX. (C) The quantitative analysis of Fig. 2B performed by ImageJ software. The results are calculated as follows: Relative fluorescence area ratio (%) = (The area with green or red fluorescence/The area with blue fluorescence) × 100. Data are mean ± SD, $n = 3$. (D) TEM images (JEM1230, JEOL, Japan) of DOX-OMV (left) and A549 cells treated with DOX-OMV for 12 h (right). Possible intracellular OMVs were visible in and around vacuoles (Arrows indicate OMVs). (E) and (F) *In vivo* drug distribution of DOX-OMV in major organs. Mice bearing A549 tumors (~ 100 mm^3) were injected a single dose of free DOX (2 μL/g), equivalent DOX loaded into OMVs or loaded into liposomes. At 1, 4 and 9 h, mice were selected randomly to obtain tumors and major organs for the investigation of DOX distribution and tumor targeting through *ex vivo* fluorescence imaging (E). Statistical analysis of fluorescence intensity (data are mean ± SD; $n = 3$) (F).

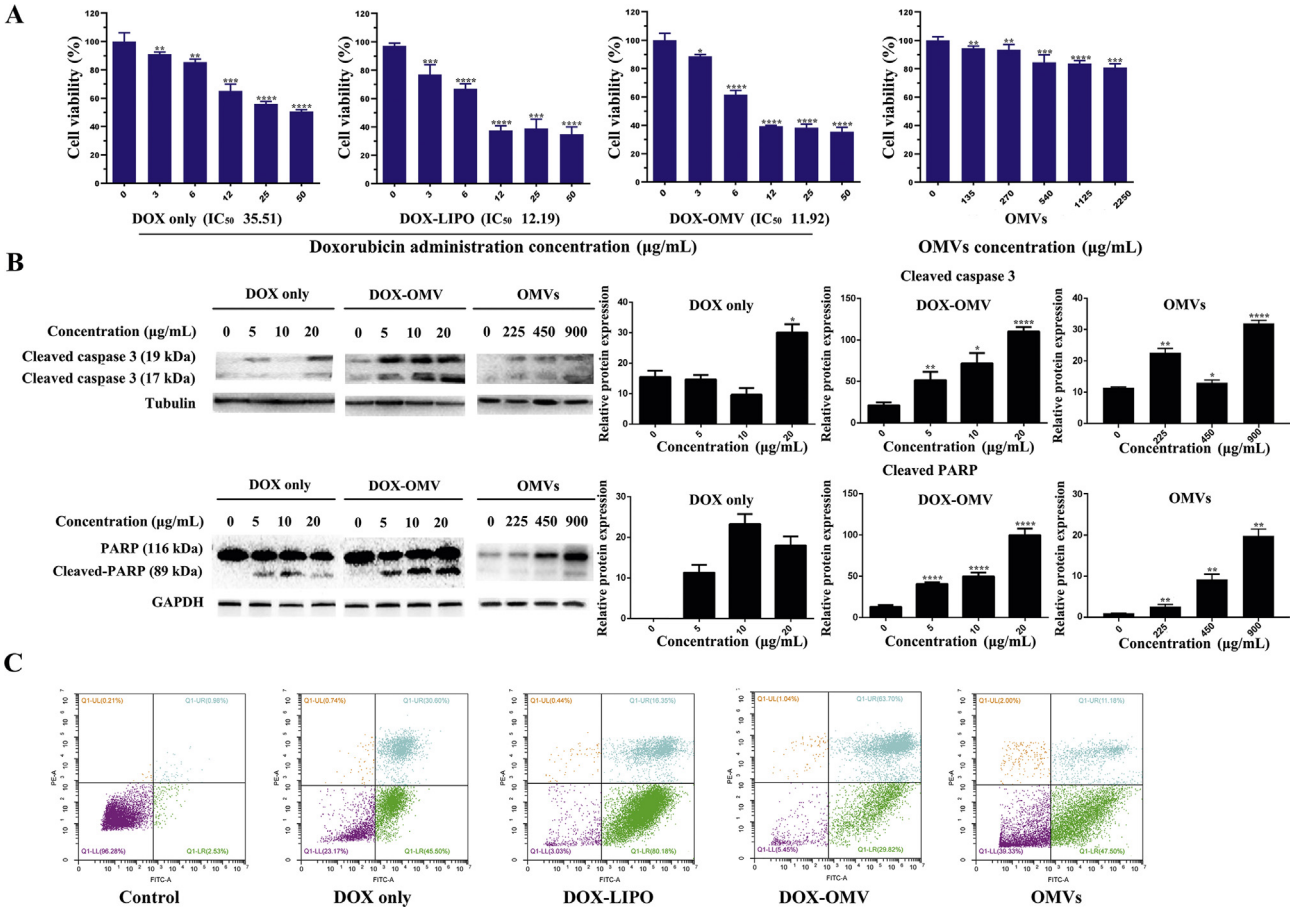

Figure 3 *In vitro* antitumor effect of DOX-OMVs. (A) A549 cells were treated with indicated concentrations of free DOX, equivalent DOX encapsulated in OMVs (DOX-OMVs) or in liposome (DOX-LIPO), and empty OMVs for 24 h. Cell viability was measured by MTT assay (IC_{50} of DOX, DOX-OMV and DOX-LIPO were 35.51, 12.19 and 11.92 μg/mL, respectively). The data were displayed as mean ± SD, $n = 5$. (B) After A549 cells were treated with indicated concentrations of OMVs, free DOX or equivalent DOX encapsulated in OMVs (DOX-OMVs), the protein levels of cleaved-caspase 3, PARP and cleaved-PARP were analyzed by Western blotting. Quantitative evaluation of the resulting bands was performed by ImageJ software. (C) A549 cells were treated with 20 μg/mL of free DOX, equivalent DOX encapsulated in OMVs (DOX-OMV) or in liposome (DOX-LIPO), and empty OMVs for 24 h, then cell apoptosis was detected by flow cytometry. $^{*}P < 0.05$, $^{**}P < 0.01$, $^{***}P < 0.001$, $^{****}P < 0.0001$ *vs.* control, $n = 3$.

Fig. S5), indicating the favorable stability of DOX-OMV *in vivo* which endowed DOX with an improved pharmacokinetic profile.

4. Discussion

Although DOX is a highly effective and broad-spectrum chemotherapy drug used in the therapy for neoplastic diseases including NSCLC, its clinical application has been limited by the dose-related cardiac toxicity such as congestive heart failure and cardiomyopathy[25]. Despite of the U.S. FDA-approval of the first PEG-coated liposomal DOX (Doxil) which brings on a substantial improvement in the therapeutic index of DOX, achieving more efficient drug delivery system and formulations with less side effects still remains a challenge. In recent years, with the boost of tumor immunotherapy, chemotherapy combined with immunotherapy draws widespread attention[26,27], especially in the treatment of lung cancer[2]. It has been recognized that activating the host immunity while chemotherapy could help to undermine residual tumor cells. A previous study have shown that the anti-lung adenocarcinoma activity of Doxil was potentiated by the combination treatment with interleukin 2 (IL-2), a lymphocyte-activating cytokine[28].

OMVs, as bilayered phospholipid nanostructures naturally released by Gram-negative bacteria, have displayed great potential as biological nanocarriers and nanoparticle-based therapeutics. OMVs have many physiological characteristics, such as the capability of adhering to host cells, carrying diverse molecules and fusing with the target cells, which make them appealing as drug-delivery vehicles[29]. Bacteria enter non-phagocytic cells through multifarious invasive and adhesive molecules, providing bacteria with an intracellular location which is considered advantageous to evade the host's immune surveillance. OMVs also share those invasive and adhesive ligands, and the adhesive properties as well as small size of OMVs allow them to escape from phagocytosis by the mononuclear phagocytes and facilitate the entry of vesicle materials to tumor cells[30]. Bioengineered OMVs with low immunogenicity from *E. coli* was used for the preparation of therapeutic siRNA-loaded OMVs, which triggered significant tumor growth inhibition through targeted gene silencing *in vivo*[18]. Recently, Huang et al.[31] developed antibiotic-loaded OMVs which could

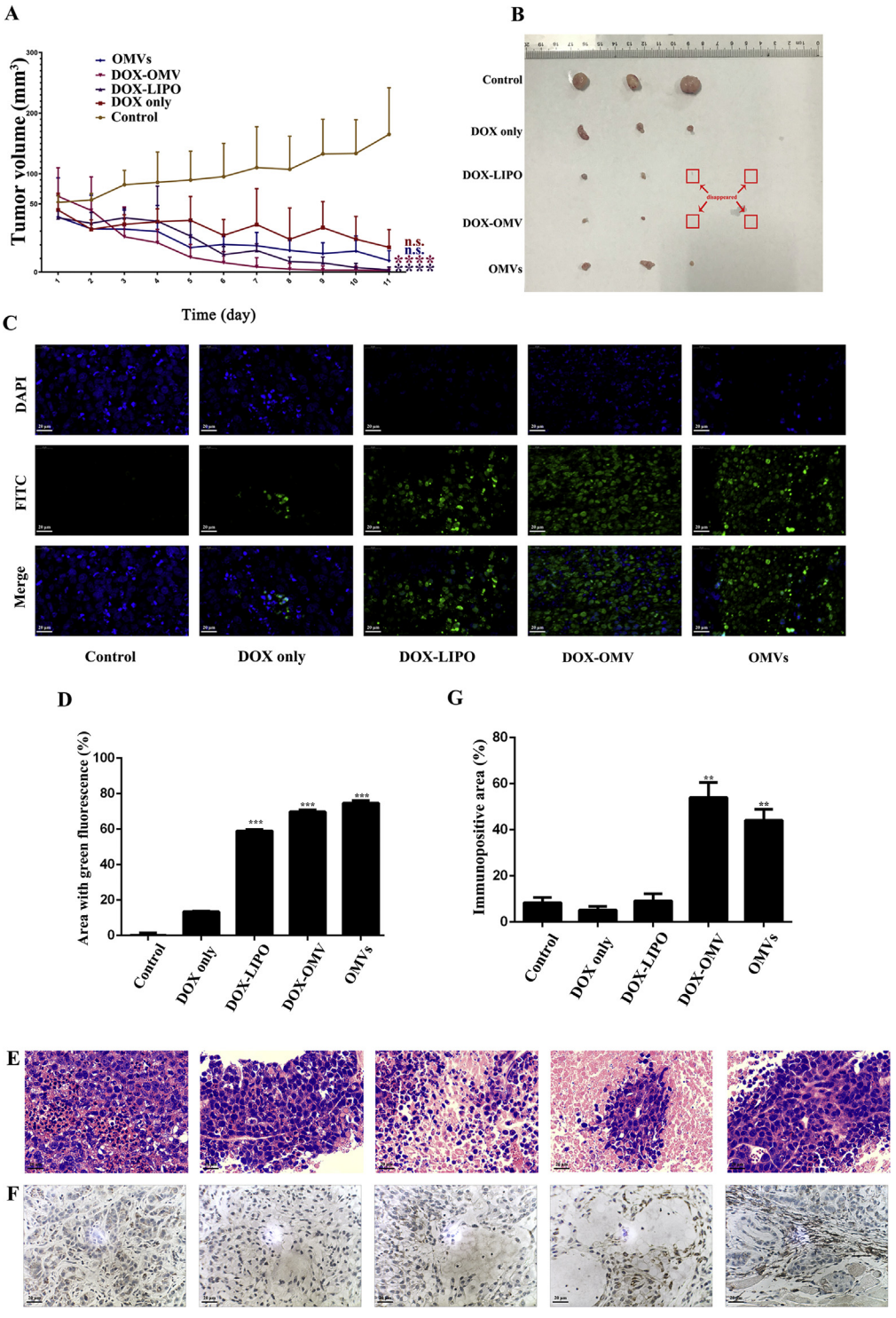

Figure 4 *In vivo* antitumor efficacy of DOX-OMV. Tumor growth suppression was investigated in A549 xenograft BALB/c mice. Mice bearing tumors (~50 mm^3) were treated (i.p. every day) with PBS, free DOX (2 mg/kg), an equivalent dose of DOX loaded into either OMVs (DOX-OMV) or liposomes (DOX-LIPO), and empty OMVs for 11 days. (A) Mean tumor volume of 5 groups. Data were displayed as mean ± SD, $n = 3$; $^{****}P < 0.001$ *vs.* control. (B) The photo of the tumor tissues removed from mice after 11 days' treatment with vehicle control ($n = 3$), free DOX ($n = 3$), DOX-OMV ($n = 4$), DOX-LIPO ($n = 4$) and empty OMVs ($n = 3$). Red boxes represent tumors disappeared in mice. (C) TUNEL assay for cell apoptosis (green fluorescence) of tumor tissues. (D) The quantitative analysis of apoptotic cells in TUNEL assay (ImageJ software). Data were displayed as mean ± SD, $n = 3$; $^{***}P < 0.001$ *vs.* control. (E) H&E staining of tumor tissue sections. (F) Immunohistochemical staining for detecting F4/80 glycoprotein in tumor sections. (G) The quantitative evaluation of immunopositive areas (ImageJ software). Data were displayed as mean ± SD, $n = 3$; $^{**}P < 0.01$ *vs.* control. Scale bar = 20 μm.

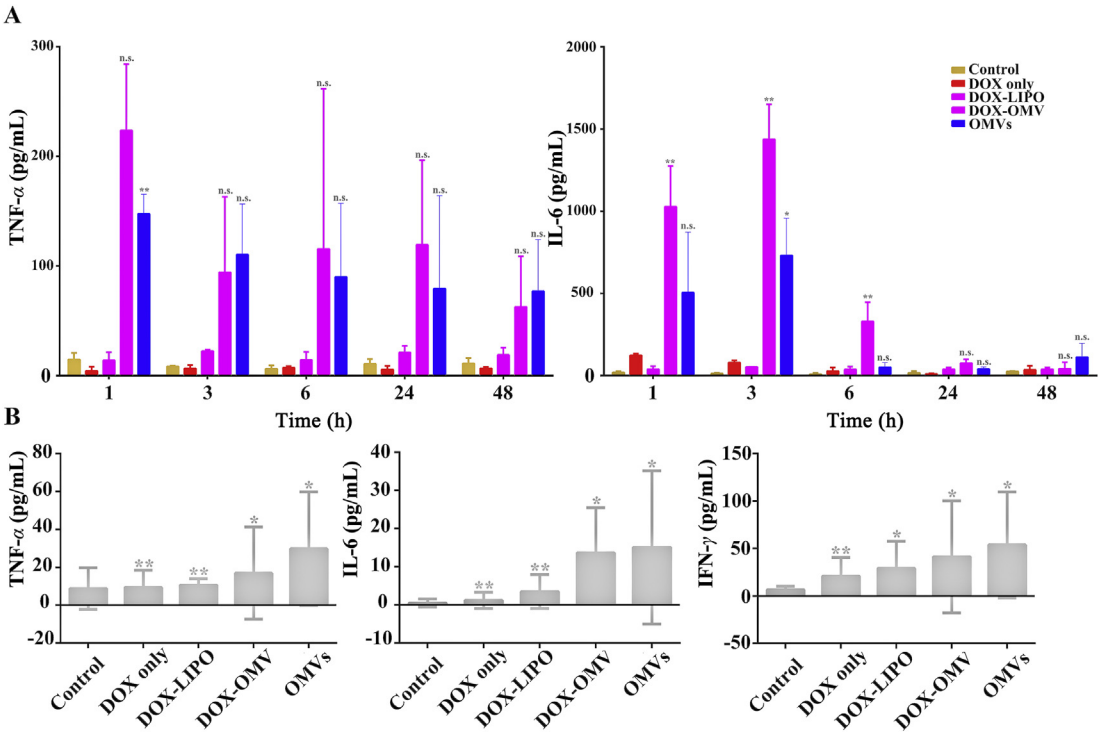

Figure 5 Serum immune cytokine analysis in C57BL/6 mice. The mice were treated (i.p. every day) with PBS, free DOX (2 mg/kg), an equivalent dose of DOX loaded into either OMVs (DOX-OMV) or liposomes (DOX-LIPO), and empty OMVs. (A) Blood sample was collected at 1, 3, 6, 24 and 48 h after initial administration, then the levels of TNF-α and IL-6 were analyzed by using respective ELISA kits. (B) After 11 days' repeated treatment, blood samples were collected and detected TNF-α, IL-6 and IFN-γ by respective ELISA kits. Data were displayed as mean $\pm$ SD, $n = 3$. $^{*}P < 0.05$, $^{**}P < 0.01$ *vs.* control. n.s. not significant.

facilitate the entry of antibiotics into pathogenic bacteria and exert a sustained bactericidal effect in the intestine with excellent biocompatibility. Besides the cargo-carrying ability, OMVs also have immuno-stimulation function[32,33]. By genetic fusion of OMV membrane molecules with subunit antigen, OMVs can be used as a vaccine-delivery system while play the role of adjuvants[20]. Although the employment of OMVs in the delivery of proteins, siRNA, microRNA and other therapeutic cargos has been achieved, whether their immunity induction function has synergistic effect with their payload to eradicate tumors remains unclear[34]. Our present study indicated that OMVs not only functioned as drug delivery carriers to facilitate the transport of chemotherapy drug DOX into tumor cells, but also elicited appropriate immune responses to enhance the anti-tumor effect of DOX with no obvious toxicity *in vivo*.

Bacterial toxicity is the main obstacle to the application of bacteria or their derived products. Recent researches have shown that some attenuated bacterial strains such as *Salmonella typhimurium* VNP20009 can be safely employed as therapeutic agents in the treatment of various tumors[35]. In this study, we adopted attenuated *K. pneumonia* to prepare OMVs. After processed by endotoxin-removing column, the obtained OMVs showed no significant cytotoxicity *in vitro* as evidenced by MTT assay and flow cytometry, as well as *in vivo* confirmed by nasal drop experiment in mice. We also investigated whether systemic administration of OMVs and their DOX-loaded agent in mice resulted in tissue disorders or death. H&E staining of organs, as well as the levels of serum biomarkers of cardiac damage including LDH, AST and CK-MB showed that this bacteria derived nanovehicles were well tolerated, and had less cardiac toxicity and no obvious damage in tissues at the experimental dose. *Ex vivo* fluorescence imaging of major organs from DOX-OMV treated mice also observed a higher level of DOX accumulation in tumor tissue and a lower level of DOX distribution in main organs especially in the heart as compared with free DOX treated mice. In addition, no significant body weight loss and mortality were found in mice after 11-days' administration. Collectively, these results, along with the improved pharmacokinetic profile of DOX-OMV, indicate that the obtained OMVs may be a promising drug-delivery vehicles. Although exosomes from mammalian cells have been investigated to be employed as naturally derived drug nanovesicles, their mass production is labor-intensive and expensive as compared with bacteria derived OMVs[21,36].

We investigated the possibility of entrapping DOX into OMVs through a gentle co-incubation approach, and the TEM and DLS analysis revealed that this method did not influence the morphology and integrity of OMVs. Moreover, LC−MS analysis confirmed the satisfactory encapsulation efficiency in appropriate proportions of OMVs and DOX, and both *in vivo* and *in vitro* drug release study displayed an ideal stability of DOX-OMV, indicating the effectiveness of this drug-carrying method.

The entry mechanisms of OMVs into host cells are diverse and have not been completely elucidated because of the species, adhesive molecules and their contents. In general, the OMVs are transported into the cells through endocytosis. In endocytosis, membrane domains invaginate, followed by being pinched off from the inner side of the cell membrane and transported within the cell. In

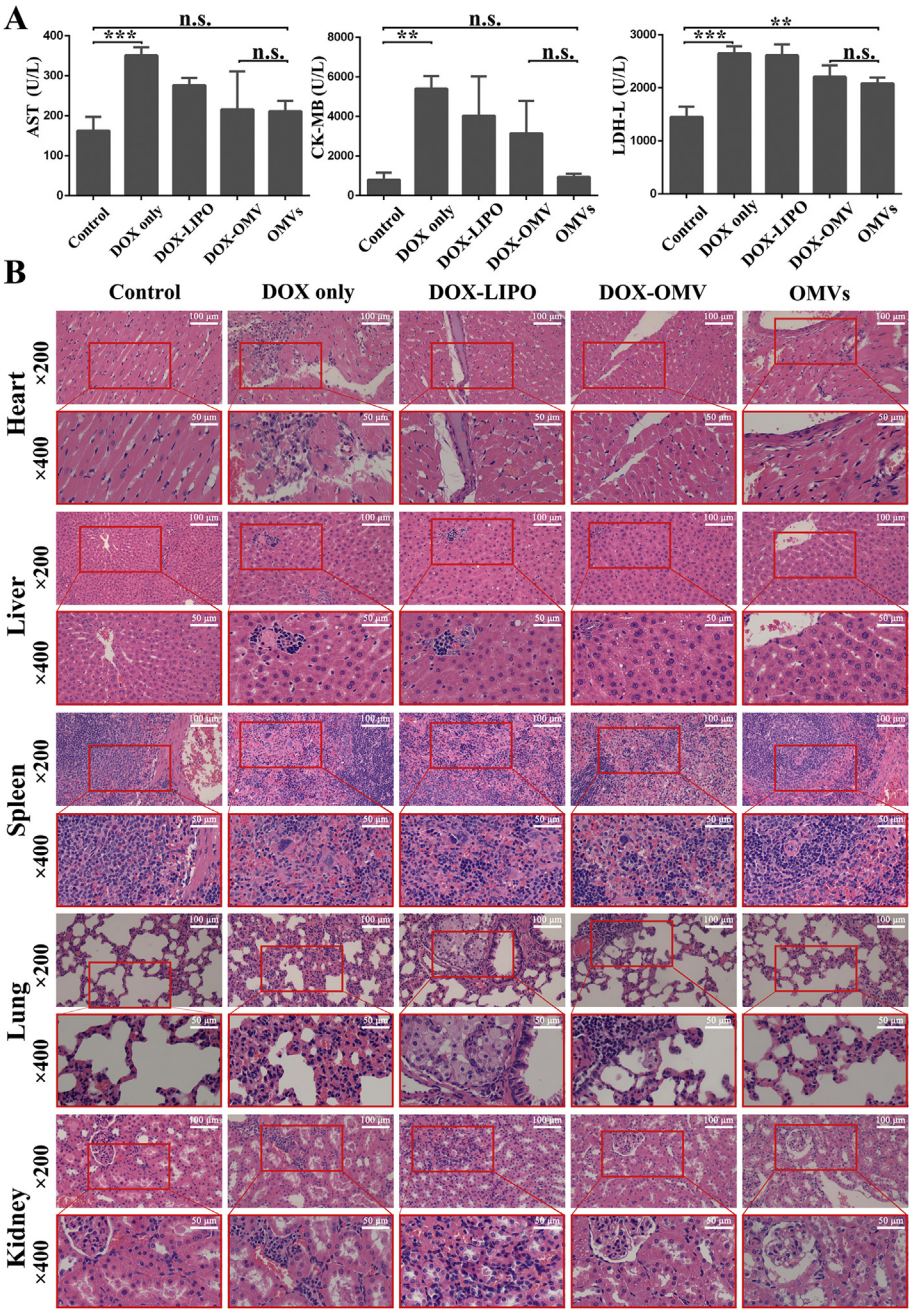

Figure 6 The safety evaluation of DOX-OMV. The tumor bearing BALB/c mice were treated as described in Fig. 4. After 11 days of treatment, various organs including heart, liver, spleen, lung and kidney together with blood samples were collected for further analysis. (A) The levels of serum biomarkers of cardiac damage including AST, CK-MB and LDH. Each bar represented mean ± SD, $n = 3$; $^{**}P < 0.01$, $^{***}P < 0.001$. n.s. not significant. (B) H&E staining of main organ sections.

addition, some OMVs are suggested to fuse with lipid rafts in the membrane and the contents are released into the cytoplasm[30]. Because DOX has intrinsic fluorescence, we then used confocal microscopy to visualize the uptake of DOX by A549 cells, and the colocalization of OMVs and DOX in tumor cells by labeling OMVs with lipophilic tracer DiO. The results revealed that OMVs carried DOX entering into A549 cells efficiently as evidenced by the accumulation of both green and red fluorescence that intensified over time inside the tumor cells. Because of their nano size, OMVs can be passively adhered to tumor cells by EPR effect, and then enter the recipient cells through endocytosis, thereby facilitating their cargos entry into cells[14]. Due to the rapid cellular uptake of DOX, DOX-OMV exerted intensive cytotoxic effects and resulted in more cell apoptosis *in vitro* as evident from MTT assay, Western blotting and flow cytometry. DOX-OMVs and DOX-LIPO have similar *in vitro* cytotoxic effects.

Our *in vivo* anti-tumor experiments also showed that DOX-OMV led to a much more substantial tumor growth inhibition,

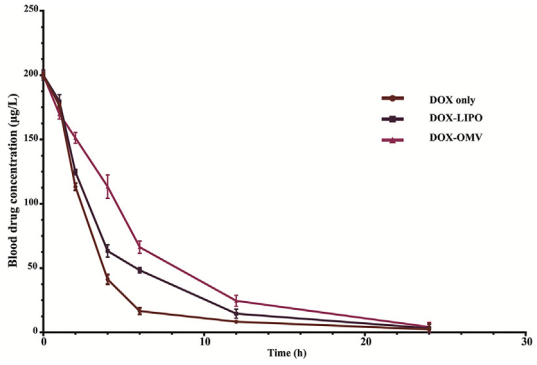

Figure 7 Pharmacokinetic profile of DOX-OMVs in rabbits. Animals were administered i.v. at doses of 1.0 mg/kg of free DOX, DOX entrapped in liposomes (DOX-LIPO) or in OMVs (DOX-OMV). Blood samples were taken at 0, 1, 2, 4, 6, 12 and 24 h after drug administration. Data were presented as mean ± SD; $n = 3$. Pharmacokinetic parameters were calculated by using DAS 2.0 software and shown in Table 1.

apoptosis and necrosis. However, there was a discrepancy between the *in vitro* and *in vivo* findings concerning to the antitumor activity of empty OMVs, which showed more tumor growth suppression and cell apoptosis than free DOX *in vivo*. It has been reported that OMVs can interact with epithelial cells directly or pattern recognition receptors to initiate immune signaling and regulate the recruitment of immune cells. OMVs also can directly interact with macrophages *in vivo* to elicit the production of pro-inflammatory cytokine by macrophages as well as activate macrophages to induce adaptive immune responses[14]. The innate immune system serves as the first line of non-specific defense against malignant cell development. Macrophages, as cells of the innate immune system, function as professional antigen presenting cells (APCs) which engulf tumor cells through phagocytosis and then activate the adaptive immune system[37]. Our further immunohistochemical analysis revealed the high level of F4/80 glycoprotein infiltration in tumor tissues of both OMVs and DOX-OMV treated mice. As F4/80 is an acknowledged marker for tissue macrophages of mouse[38], these findings suggest that OMVs could induce macrophage-mediated antitumor immunity efficacy which might synergize with their cargo DOX in BALB/c nude mice[39]. Moreover, in C57BL/6 mice treated with OMVs or DOX-OMVs, after a rapid rise in the first few hours, the serum cytokine (IL-6, TNF-α or IFN-γ) level returned and maintained at a level slightly higher than that of the control group. This phenomenon is in accordance with previous report and further proved the favorable tolerability and safety profile of OMVs[18]. However, whether the appropriate higher immune responses than normal could elicit anti-tumor immunological effect and synergize with their cargos needs to be further investigated in C57BL/6 mice.

In conclusion, our study illustrates that the attenuated *K. pneumonia* derived OMVs, as a kind of biological drug-delivery carriers, are highly effective in transporting the chemotherapy drug DOX into NSCLC A549 cells. In addition, they can elicit appropriate immune responses, thereby enhancing the anti-tumor effect of DOX with no obvious toxicity in *vivo* (Fig. 8). Thus, OMVs entrapping chemotherapeutic agents is a potential chemoimmunotherapy strategy for cancer control.

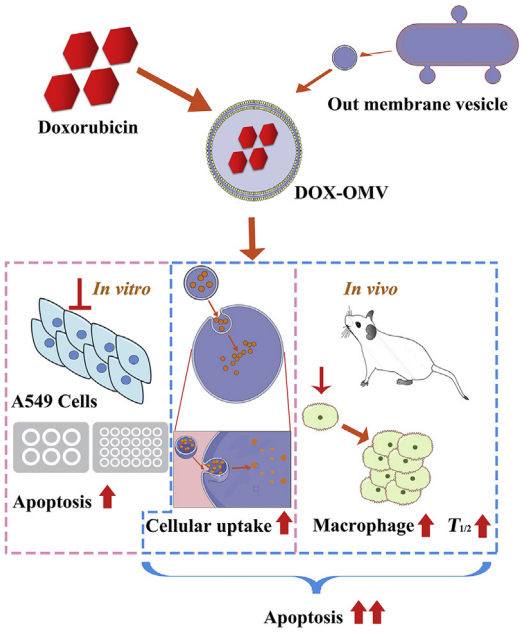

Figure 8 Overview of anti-NSCLC effect triggered by DOX-OMV. *In vitro*, DOX encapsulated in OMVs was efficiently delivered into A549 cells, thus resulted in intensive cytotoxic effects and cell apoptosis. *In vivo*, OMVs not only functioned as drug delivery carriers but also induced the recruitment of macrophages in tumor microenvironment which might synergize with their cargo DOX.

Table 1 Pharmacokinetic parameters of doxorubicin administered to animals as the free drug (doxorubicin) or entrapped in liposome and OMVs.

Animal species/drug form	Dose (mg/kg)	C_{max} (mg/L)	AUC (mg·h/L)		$t_{1/2}$ (h)			MRT (h)		CL (mL/h/kg)[a]
			AUC_{0-24}	$AUC_{0-\infty}$	$t_{1/2\alpha}$	$t_{1/2\beta}$	$t_{1/2\gamma}$	MRT_{0-24}	$MRT_{0-\infty}$	
Free DOX	1	200	684.125	705.888	2.035	2.035	2.174	3.631	4.554	1.536231644
DOX-LIPO	1	200	936.594	957.635	2.648	2.648	69.315	4.534	5.107	1.084469445
DOX-OMV	1	200	1234.364	1259.543	4.177	4.177	69.315	5.657	22.281	0.785820863

AUC = area under the concentration−time curve; CL = total plasma body clearance; C_{max} = peak plasma concentration after single dose administration; $t_{1/2}$ = drug metabolism half-life.

[a]For weight normalization of CL, average rabbit weights were estimated at 2 kg.

Acknowledgments

This study was sponsored by Scientific and Innovative Action Plan of Shanghai (No. 18431902800, China), National Natural Science Foundation of China (No. 81572979), Project of Shanghai Health and Family Planning Commission (201940102, China) and National Key Basic Research Program of China (2015CB931800).

Author contributions

Kudelaidi Kuerban and Xiwen Gao conducted the experiments and wrote the manuscript with equal contribution. Hui Zhang was responsible for confocal microscopy and Western blot. Jiayang Liu and Mengxue Dong participated in immunohistochemistry and flow cytometry. Ruihong Ye took part in the *in vivo* experiments. Lina Wu and Meiqing Feng analyzed the data and revised the manuscript. Li Ye designed the research plan, analyzed the data and revised the manuscript. All authors have approved the manuscript.

Conflicts of interest

The author declare no conflicts of interest.

Appendix A. Supporting information

Supporting data to this article can be found online at https://doi.org/10.1016/j.apsb.2020.02.002.

References

1. Bray F, Ferlay J, Soerjomataram I, Siegel RL, Torre LA, Jemal A. Global cancer statistics 2018: GLOBOCAN estimates of incidence and mortality worldwide for 36 cancers in 185 countries. *Ca - Cancer J Clin* 2018;**68**:394−424.
2. Zappa C, Mousa SA. Non-small cell lung cancer: current treatment and future advances. *Transl Lung Cancer Res* 2016;**5**:288−300.
3. Tacar O, Sriamornsak P, Dass CR. Doxorubicin: an update on anticancer molecular action, toxicity and novel drug delivery systems. *J Pharm Pharmacol* 2013;**65**:157−70.
4. O'Brien ME, Wigler N, Inbar M, Rosso R, Grischke E, Santoro A, Catane RD, Tomczak P, Orlandi F, Mellars L, Alland L, TendlerM C, O'Brien E, Wigler N, Inbar M, Rosso R, Grischke E, Santoro A, Catane R, Kieback DG, Tomczak P, Ackland SP, Orlandi F, Mellars L, Alland L, Tendler C. Reduced cardiotoxicity and comparable efficacy in a phase III trial of pegylated liposomal doxorubicin HCl (CAELYX™/Doxil®) *versus* conventional doxorubicin for first-line treatment of metastatic breast cancer. *Ann Oncol* 2004;**15**:440−9.
5. Barenholz Y. Doxil® — the first FDA-approved nano-drug: lessons learned. *J Contr Release* 2012;**160**:117−34.
6. Lotem M, Hubert A, Lyass O, Goldenhersh MA, Ingber A, Peretz T, et al. Skin toxic effects of polyethylene glycol-coated liposomal doxorubicin. *Arch Dermatol* 2000;**136**:1475−80.
7. Gabizon A, Shmeeda H, Barenholz Y. Pharmacokinetics of pegylated liposomal doxorubicin. *Clin Pharmacokinet* 2003;**42**:419−36.
8. Knudsen KB, Northeved H, Kumar Ek P, Permin A, Gjetting T, Andresen TL, et al. *In vivo* toxicity of cationic micelles and liposomes. *Nanomed Nanotechnol Biol Med* 2015;**11**:467−77.
9. Yoo JW, Irvine DJ, Discher DE, Mitragotri S. Bio-inspired, bioengineered and biomimetic drug delivery carriers. *Nat Rev Drug Discov* 2011;**10**:521.
10. Schwechheimer C, Kuehn MJ. Outer-membrane vesicles from Gram-negative bacteria: biogenesis and functions. *Nat Rev Microbiol* 2015;**13**:605.
11. Berleman J, Auer M. The role of bacterial outer membrane vesicles for intra- and interspecies delivery. *Environ Microbiol* 2013;**15**:347−54.
12. Jan AT. Outer membrane vesicles (OMVs) of Gram-negative bacteria: a perspective update. *Front Microbiol* 2017;**8**:1053.
13. Vanaja Sivapriya K, Russo Ashley J, Behl B, Banerjee I, Yankova M, et al. Bacterial outer membrane vesicles mediate cytosolic localization of LPS and caspase-11 activation. *Cell* 2016;**165**:1106−19.
14. Kaparakis-Liaskos M, Ferrero RL. Immune modulation by bacterial outer membrane vesicles. *Nat Rev Immunol* 2015;**15**:375.
15. Gnopo YM, Watkins HC, Stevenson TC, DeLisa MP, Putnam D. Designer outer membrane vesicles as immunomodulatory systems—reprogramming bacteria for vaccine delivery. *Adv Drug Deliv Rev* 2017;**114**:132−42.
16. Holst J, Martin D, Arnold R, Huergo CC, Oster P, O'Hallahan J, et al. Properties and clinical performance of vaccines containing outer membrane vesicles from Neisseria meningitidis. *Vaccine* 2009;**27**:B3−12.
17. Andrews SM, Pollard AJ. A vaccine against serogroup B Neisseria meningitidis: dealing with uncertainty. *Lancet Infect Dis* 2014;**14**:426−34.
18. Gujrati V, Kim S, Kim SH, Min JJ, Choy HE, Kim SC, et al. Bioengineered bacterial outer membrane vesicles as cell-specific drug-delivery vehicles for cancer therapy. *ACS Nano* 2014;**8**:1525−37.
19. Klimentova J, Stulik J. Methods of isolation and purification of outer membrane vesicles from Gram-negative bacteria. *Microbiol Res* 2015;**170**:1−9.
20. Chen DJ, Osterrieder N, Metzger SM, Buckles E, Doody AM, DeLisa MP, et al. Delivery of foreign antigens by engineered outer membrane vesicle vaccines. *Proc Natl Acad Sci U S A* 2010;**107**:3099−104.
21. Tian Y, Li S, Song J, Ji T, Zhu M, Anderson GJ. A doxorubicin delivery platform using engineered natural membrane vesicle exosomes for targeted tumor therapy. *Biomaterials* 2014;**35**:2383−90.
22. Kesty NC, Mason KM, Reedy M, Miller SE, Kuehn MJ. Enterotoxigenic *Escherichia coli* vesicles target toxin delivery into mammalian cells. *EMBO J* 2004;**23**:4538−49.
23. Lin HH, Faunce DE, Stacey M, Terajewicz A, Nakamura T, Zhang-Hoover J. The macrophage F4/80 receptor is required for the induction of antigen-specific efferent regulatory T cells in peripheral tolerance. *J Exp Med* 2005;**201**:1615−25.
24. Kim SW, Kim JS, Papadopoulos J, Choi HJ, He J, Maya M. Consistent interactions between tumor cell IL-6 and macrophage TNF-alpha enhance the growth of human prostate cancer cells in the bone of nude mouse. *Int Immunopharm* 2011;**11**:862−72.
25. Wu S, Ko YS, Teng MS, Ko YL, Hsu LA, Hsueh C, et al. Adriamycin-induced cardiomyocyte and endothelial cell apoptosis: *in vitro* and *in vivo* studies. *J Mol Cell Cardiol* 2002;**34**:1595−607.
26. Mellman I, Coukos G, Dranoff G. Cancer immunotherapy comes of age. *Nature* 2011;**480**:480−9.
27. Kelly PN. The cancer immunotherapy revolution. *Science* 2019;**359**:1344−5.
28. Cabanes A, Even-Chen S, Zimberoff J, Barenholz Y, Kedar E, Gabizon A. Enhancement of antitumor activity of polyethylene glycol-coated liposomal doxorubicin with soluble and liposomal interleukin 2. *Clin Canc Res* 1999;**5**:687−93.
29. Toyofuku M, Tashiro Y, Hasegawa Y, Kurosawa M, Nomura N. Bacterial membrane vesicles, an overlooked environmental colloid: biology, environmental perspectives and applications. *Adv Colloid Interface Sci* 2015;**226**:65−77.
30. Amano A, Takeuchi H, Furuta N. Outer membrane vesicles function as offensive weapons in host−parasite interactions. *Microb Infect* 2010;**12**:791−8.
31. Huang W, Zhang Q, Li W, Yuan M, Zhou J, Hua L. Development of novel nanoantibiotics using an outer membrane vesicle-based drug efflux mechanism. *J Contr Release* 2019;**317**:1−22.
32. Gerritzen MJH, Martens DE, Wijffels RH, van der Pol L, Stork M. Bioengineering bacterial outer membrane vesicles as vaccine platform. *Biotechnol Adv* 2017;**35**:565−74.
33. Kuipers K, Daleke-Schermerhorn MH, Jong WS, ten Hagen-Jongman CM, van Opzeeland F, Simonetti E. *Salmonella* outer membrane vesicles

displaying high densities of pneumococcal antigen at the surface offer protection against colonization. *Vaccine* 2015;**33**:2022−9.
34. Raposo G, Stoorvogel W. Extracellular vesicles: exosomes, microvesicles, and friends. *J Cell Biol* 2013;**200**:373−83.
35. Zheng JH, Nguyen VH, Jiang SN, Park SH, Tan W, Hong SH, et al. Two-step enhanced cancer immunotherapy with engineered *Salmonella typhimurium* secreting heterologous flagellin. *Sci Transl Med* 2017;**9**:eaak9537.
36. Corrado C, Raimondo S, Chiesi A, Ciccia F, De Leo G, Alessandro R. Exosomes as intercellular signaling organelles involved in health and disease: basic science and clinical applications. *Int J Mol Sci* 2013;**14**:5338−66.
37. Feng M, Jiang W, Kim BY, Zhang CC, Fu YX, Weissman IL. Phagocytosis checkpoints as new targets for cancer immunotherapy. *Nat Rev Canc* 2019;**19**:568−86.
38. Gordon S, Hamann J, Lin HH, Stacey M. Celebrating 30 years F4/80 and the related adhesion-GPCRs. *Eur J Immunol* 2011;**41**:2472−6.
39. Zhang X, Fan J, Wang S, Li Y, Wang Y, Li S, et al. Targeting CD47 and autophagy elicited enhanced antitumor effects in non-small cell lung cancer. *Cancer Immunol Res* 2017;**5**:363−75.